Journal of Molecular Structure xxx (xxxx) xxx

Contents lists available at ScienceDirect

Journal of Molecular Structure

journal homepage: www.elsevier.com/locate/molstr

Mildness in preparative conditions directly affects the otherwise straightforward syntheses outcome of Schiff-base isoniazid derivatives: Aroylhydrazones and their solvolysis-related dihydrazones

Daphne S. Cukierman[a,*], Beatriz N. Evangelista[a], Carlos Castanho Neto[b], Chris H.J. Franco[c], Luiz Antônio S. Costa[d], Renata Diniz[e], Jones Limberger[b], Nicolás A. Rey[a,*]

[a] Laboratório de Síntese Orgânica e Química de Coordenação Aplicada a Sistemas Biológicos (LABSO-Bio), Departamento de Química, Pontifícia Universidade Católica do Rio de Janeiro, Rio de Janeiro, 22451-900, Brazil
[b] Laboratório de Síntese Orgânica e Química Fina (LaSOQF), Departamento de Química, Pontifícia Universidade Católica do Rio de Janeiro, Rio de Janeiro, 22451-900, Brazil
[c] Departamento de Química, Campus Martelos, Universidade Federal de Juiz de Fora, Juiz de Fora, 36036-900, Brazil
[d] Núcleo de Estudos em Química Computacional (NEQC), Departamento de Química, ICE, Universidade Federal de Juiz de Fora, Juiz de Fora, 36036-900, Brazil
[e] Grupo de Cristalografia Química (GCQ), Departamento de Química, ICEx, Universidade Federal de Minas Gerais, Belo Horizonte, 31270-901, Brazil

ARTICLE INFO

Article history:
Received 28 June 2020
Revised 27 September 2020
Accepted 9 October 2020
Available online xxx

Keywords:
Aroylhydrazones
Dihydrazones
Isoniazid
Solvolysis
Hirshfeld surfaces

ABSTRACT

Aroylhydrazones are versatile compounds with a series of applications, from biological to technological spheres. The simplicity of their preparation allows for a great chemical variability and synthetic manageability. However, the process can be not as straightforward as one would imagine. Some parameters such as specific reactants, the amount of acid employed as catalyst and reaction temperature can have a direct impact on the obtained product. In the present work, we describe two series of novel isoniazid-derived compounds prepared from a pair of different aldehyde precursors, as well as the solvolysis, under harsh synthetic conditions, of the initially formed aroylhydrazones, leading to unexpected dihydrazones. All compounds were unequivocally characterized in solution using 1D and 2D NMR experiments in DMSO–d_6 and, in the solid-state, by other classic techniques. System I is composed by 2-(1H-pyrazol-1-yl)benzaldehyde and its hydrazone derivatives, while system II comprises 2-(4-metoxyphenoxy)benzaldehyde and its related Schiff-base products. The first aldehyde was obtained for the first time *via* the copper-catalyzed Ullmann C–N coupling between 2-bromobenzaldehyde and pyrazole. Single crystals of its aroylhydrazone and dihydrazone derivatives were isolated and thoroughly characterized, including Hirshfeld surfaces and energy frameworks studies. Finally, we describe an NMR and theoretically-based proposed reaction pathway for the unexpected formation of the dihydrazones involving the solvolysis of the initially formed isonicotinoyl hydrazone followed by attack to a second free aldehyde molecule.

1. Introduction

Aldehyde-derived hydrazones compose an organic class of compounds which present, in their structures, the functional group $R_1HC{=}N{-}NR_2R_3$. In hydrazones, the azomethine C=N double bond is conjugated with the electron pair of the neighboring nitrogen, which makes them more resistant to hydrolysis than common Schiff bases. Hydrazones, synthesized through the condensation reaction between hydrazides and carbonyl compounds, are particularly interesting in medicinal chemistry and have been identified as important hits and lead compounds to act upon different molecular targets [1]. They have been employed in a wide spectrum of pharmacological applications [2], such as analgesics [3], anti-inflammatories [4], anti-tuberculosis [5], antitumor agents [6] and antimalarials [7]. Specifically, *N*-acylhydrazones have also been the subject of several studies in the inorganic chemistry field due to the presence of the $R_1R_2C{=}N{-}NH{-}CO{-}$ moiety, which allows them to perform as bidentate ligands, coordinating metal ions through the azomethine nitrogen and the carbonyl oxygen. For example, these compounds have been investigated as iron chelators for the control of neurodegenerative disorders such as Friedreich ataxia and other diseases related to the excess of this metal

* Corresponding authors:.
E-mail addresses: daphcukierman@gmail.com (D.S. Cukierman), nicoarey@puc-rio.br (N.A. Rey).

https://doi.org/10.1016/j.molstruc.2020.129437
0022-2860/

[8–10]. In this scenario, *ortho*-pyridine-derived isonicotinoyl hydrazones are of interest, since they can efficiently bind mitochondrial iron through the tridentate N_{py}, N, O-chelating system [11].

Our research group at the Department of Chemistry of the Pontifical Catholic University of Rio de Janeiro specializes in the synthesis, characterization and application of different hydrazones and their metal complexes, for a series of purposes ranging from technological to pharmacological applications [12–23]. For example, we have explored the luminescent properties of a symmetric dihydrazone and its possible use as a constituent of the emitting layer for the fabrication of OLEDs [16]. We have also shown that a series of dinuclear copper(II) complexes covering different hydrazonic ligands display potent antiproliferative activity against a panel of several cancer cell lines [21,22]. Our efforts have been focused towards neurodegenerative disorders too, such as Alzheimer's and Parkinson's diseases, since we have observed that isonicotinoyl hydrazones constitute a promising class of Metal-Protein Attenuating Compounds (MPACs) acting as selective ligands for biometal-binding according to the metal hypothesis of these disorders [13,14,18,19,23]. Moreover, we have just demonstrated the ability of these compounds in preventing the metal-catalyzed oxidation of a mutant fragment of human prion protein [20].

Our lead compound, i.e., 8-hydroxyquinoline-2-carboxaldehyde isonicotinoyl hydrazone (INHHQ), is capable of competing, in vitro, for the interactions of Zn^{2+} and Cu^{2+} with the Aβ peptide [14]. *In silico* pharmacological analyses demonstrated that the compound is neutral in physiological pH and it is capable of crossing the blood-brain barrier, which has recently been proved through its detection, by HPLC, in the brains of Wistar rats intraperitoneally injected with INHHQ [18]. Despite the presence of the 8-hydroxyquinoline (8-HQ) moiety, traditionally used in the synthesis of new MPACs described in recent literature, we suggested that the Zn^{2+} and Cu^{2+} coordination in INHHQ occurs through the aroylhydrazonic system, an innovation that opens new perspectives regarding the development of hydrazones as potential MPACs.

However, in spite of the apparent simplicity related to the one-step synthesis of hydrazones, which partially accounts for the broad range of applications discussed above, some systems are not so straightforward. In this context, the current work reports on the preparation of two novel isonicotinoyl (isoniazid-derived) hydrazones, obtained from 2-(1H-pyrazol-1-yl)benzaldehyde and 2-(4-metoxyphenoxy)benzaldehyde. We observed that, depending on the "mildness degree" of the experimental conditions employed (pH, temperature), a dihydrazone solvolysis product can take over as the main product of the reaction. All the six compounds (aldehydes, aroylhydrazones and dihydrazones) were unequivocally characterized in the solid-state, by means of a series of classic techniques, as well as in solution (using uni- and bidimensional NMR experiments in DMSO–d_6). Single crystals adequate to structural elucidation through XRD were obtained for the aroylhydrazone and the dihydrazone derived from 2-(1H-pyrazol-1-yl)benzaldehyde and their structures are also discussed, along with their Hirshfeld surfaces description. Also, a reaction pathway for the conversion of isonicotinoyl hydrazones into dihydrazones in strong acidic medium and under reflux is suggested and has been studied through ^{1}H NMR experiments for the 2-(4-metoxyphenoxy)benzaldehyde derivatives. Theoretical calculations were employed to obtain thermodynamic support for this proposition.

2. Materials and methods

2.1. Syntheses

Chemicals and solvents were obtained from commercial sources and used without further purification with the exception of DMF employed in the Ullmann reactions, which was degassed before use. Reactions monitored by TLC were performed on Macherey-Nagel Alugram® Sil 60/UV_{254} sheets (thickness 0.2 mm). Purification of products was carried out by column chromatography using Macherey-Nagel silica gel (230–400 mesh).

2.1.1. Synthesis of 2-(1H-pyrazol-1-yl)benzaldehyde (1) via *Ullmann coupling*

An oven-dried resealable Schlenk flask was charged with 2-bromobenzaldehyde (1.5 mmol), pyrazole (2.25 mmol), CuI (0.15 mmol) and K_3PO_4 (3.0 mmol), evacuated and back-filled with nitrogen. Then, degassed DMF (8.0 mL) was added and the reaction mixture was stirred at 75 °C for 24 h. After this period, the solution was allowed to cool-down to room temperature, diluted with 20 mL of ethyl acetate and washed with deionized water (3 × 7 mL). The organic layer was dried over Na_2SO_4, filtered and concentrated in vacuum. After column chromatography (eluent: hexane – ethyl acetate 6:1), the desired product **1** was obtained as a white solid (53% yield). M.p.: 55–57 °C. GC–MS (EI, 70 eV) *m/z* (%): 171(1), 144(100), 117(25), 104(7), 90(30), 77(35).

2.1.2. Synthesis of 1,2-bis[2-(1*H*-pyrazol-1-yl)benzylidene]*hydrazone (2)*

Compound **2**, a dihydrazone, was unexpectedly obtained in the form of single crystals from the slow evaporation of the mother liquor in an attempt of synthesizing the 2-(1H-pyrazol-1-yl)benzaldehyde isonicotinoyl hydrazone (inhere called compound **3**). In this synthesis, 0.5 mmol of isoniazid (isonicotinic acid hydrazide) in 10.0 mL of ethanol was dropwise added to 5.0 mL of an ethanolic solution containing 0.5 mmol of **1**. The reaction mixture was kept under reflux for 3 h and no precipitation was observed upon cooling of the solution. Thus, 3 drops of conc. hydrochloric acid were added to the mixture, which immediately turned bright yellow. It was then refluxed for another 3 h. When performed under such conditions, compound **2** was the only isolated product after slow evaporation of the solvent.

To synthesize compound **2** in higher yields, another route involving hydrazine as one of the starting materials was attempted. Free hydrazine was obtained from hydrazine dihydrochloride (0.25 mmol in 5 mL of methanol) by its neutralization with potassium hydroxide (0.25 mol L^{-1} methanolic solution), after filtrating the KCl precipitate. To the resulting solution, 0.5 mmol of **1**, dissolved in 5 mL of methanol, was dropwise added and the yellow mixture was left stirring for 4 h at room temperature. Compound **2** was isolated after slow evaporation of the solvent (65% yield). M.p.: 159–161 °C.

2.1.3. Synthesis of 2-(1H-pyrazol-1-yl)benzaldehyde isonicotinoyl hydrazone (3)

To a solution of **1** (0.5 mmol in 5.0 mL of ethanol), an ethanolic solution of isoniazid (0.5 mmol in 10.0 mL) was dropwise added. Upon addition of 1 drop of conc. hydrochloric acid, the mixture turned bright yellow. It was then left stirring for 4 h at room temperature. Single crystals of compound **3** suitable for X-ray diffraction analysis were obtained after slowly concentrating the solution (51% yield). M.p. 154–157 °C.

2.1.4. Synthesis of 2-(4-metoxyphenoxy)benzaldehyde (4)

A mixture of 4-methoxyphenol (2.75 mmol), 2-fluorobenzaldehyde (2.50 mmol), K_2CO_3 (3.00 mmol) and DMF (5 mL) was stirred in a resealable Schlenk flask at 150 °C for 4 h. Then, the reaction mixture was allowed to cool down, diluted with 20 mL of ethyl acetate and washed with 1.0 mol L^{-1} potassium hydroxide and water (3 × 7 mL). The organic layer was dried over Na_2SO_4, filtered and concentrated under vacuum, affording the aldehyde (compound **4**) as a pale yellow solid (71% yield) [24,25]. M. p. 63–65 °C.

2.1.5. Synthesis of 1,2-bis[2-(4-methoxyphenoxy) benzylidene]hydrazone (5)

To evaluate whether the reaction between aldehyde **4** and isoniazid under harsh synthetic conditions would afford the dihydrazonic product as reported for the previous case, 5.0 mL of an ethanolic solution containing 0.2 mmol of isoniazid were dropwise added to another 5.0 mL of an equimolar ethanolic solution of **4**. No change in the color of the solution was observed. Thus, 3 drops of conc. hydrochloric acid were added. The solution immediately turned bright yellow and precipitation occurred. The system was kept under reflux for a period of 3 h, which re-dissolved the precipitate. Upon cooling and slow evaporation of the solvent, a yellow solid was isolated.

Alternatively, hydrazine dihydrochloride (0.125 mmol in 2.5 mL of methanol) was reacted with potassium hydroxide (0.25 mol L^{-1} methanolic solution) to obtain the free hydrazine, after separating the KCl precipitate. To the resultant filtrate, 0.25 mmol of **4** in methanol (2.5 mL) was dropwise added resulting in the immediate formation of a light yellow precipitate corresponding to compound **5**. Stirring was kept for additional 40 min before filtration in a glass funnel (60% yield). M.p. 166–167 °C.

2.1.6. Synthesis of 2-(4-metoxyphenoxy)benzaldehyde isonicotinoyl hydrazone (6)

This isonicotinoyl hydrazone was prepared similarly to compound **3**, in a Schiff base condensation reaction. A solution containing isoniazid (0.25 mmol in 6.0 mL of ethanol) was dropwise added to an ethanolic solution of **4** (0.25 mmol in 5.0 mL). One drop of conc. hydrochloric acid was added as catalyst and the solution immediately turned bright yellow. No precipitation was observed and the reaction mixture was kept under stirring for 3 h at room temperature. Slow evaporation of the solvent afforded a bright yellow precipitate (compound **6**, 83% yield). M.p. 216–218 °C.

2.2. Instrumentation and characterization

Melting points were determined either on a Büchi SMP-20 capillary apparatus or in a Fisatom model 431 apparatus. Thermogravimetric studies, on the other hand, were conducted in a Perkin-Elmer analyzer, model Pyris 1 TGA, under nitrogen atmosphere, in the range 25–900 °C, using a heating rate of 10 °C min^{-1}. FT-IR spectra were recorded on a Perkin-Elmer 100 FT-IR spectrometer in KBr. Mass spectra were obtained on a GC/MS Shimadzu QP-5050 (EI, 70 eV) equipped with a 30 meter DB-5MS column. NMR spectra were recorded on a Bruker Avance III HD-400 spectrometer (operating at 400 MHz for ^{1}H and 100 MHz for ^{13}C). Chemical shifts are expressed in ppm relative to tetramethylsilane (TMS) and the spectra were calibrated based on the residual solvent signal (quintet at 2.50 ppm for ^{1}H and septet at 39.52 for ^{13}C).

The single crystal X-ray diffraction data for **2** and **3** were collected in an Agilent-Rigaku Supernova diffractometer using MoKα (λ = 0.71073 Å) radiation at room temperature (293 K). The data collection, cell refinements and data reduction were performed using the CRYSALISPRO software [26]. The structures were resolved by direct methods using SIR [27] program and refined by SHELXL-2018/3 [28] using the WinGX system [29]. All non-hydrogen atoms were refined with anisotropic thermal parameters. H atoms connected to carbon were placed in idealized positions and treated by rigid model, with Uiso(H) = 1.2 Ueq for aromatic rings and CH groups. In compound **3**, the hydrazone-related NH group was treated similarly to CH groups. Figures were drawn using ORTEP-3 for Windows [30], Pov-Ray [31] and Mercury [32] programs. The analysis of Hirshfeld surfaces, fingerprint plots and energy frameworks were performed through the CrystalExplorer program [33].

2.3. Theoretical calculations

The optimization and harmonic frequencies of the hydrazonic derivatives **2, 3, 5** and **6** have been conducted using the Stefan Grimme's Hartree-Fock-3c (HF-3c) method, developed as an option to achieve good and reliable results in reduced, very convenient, computational time [34]. For all structures, the level of theory applied was HF MINIX D3BJ GCP(HF/MINIX), i.e., which contemplates corrections for basis set superposition error (BSSE) by the geometric counterpoise scheme (gCP) [35], atom-pairwise dispersion correction with the Becke-Johnson damping scheme (D3BJ) [36,37] and a correction for short-range basis incompleteness (nine empirical parameters are used overall). Also, this method was applied to provide the energetic pathway for the mechanistic investigation involving compounds **5** and **6**. This method was used on ORCA 3.0.3 release [38].

The density functional theory (DFT) approach was also employed with the well-established level of theory CAM-B3LYP/6–311+*G*(2d,p) [39, 40] in order to confirm the assigned vibrational modes. All calculations were performed at 298 K and 1 atm in gas phase. DFT calculations were carried out on the Gaussian 09 software package [41]. All calculations were performed on Dell servers from NEQC, UFJF.

2.4. ^{1}H NMR measurements to follow the reaction pathway in system II

Mechanistic insights on the unexpected formation of the dihydrazones **2** and **5** under severe synthetic conditions were obtained from system II, involving the reaction between aldehyde **4** and isoniazid. Samples (20 μL) from the reaction mixture were taken in three different synthetic steps: immediately after the mixture of both reagents (step 1), after the addition of conc. hydrochloric acid (step 2) and after 3 h of reaction under reflux (step 3). These aliquots were diluted to 600 μL with DMSO–d_6 and added to 5 mm NMR tubes and a ^{1}H NMR spectrum of each sample was recorded.

3. Results and discussion

3.1. 2-(1H-pyrazol-1-yl)benzaldehyde-derived compounds (system I)

Two different strategies were employed in the synthesis of aldehyde **1** (Scheme 1). Initially, 2-fluorobenzaldehyde was reacted with pyrazole in the presence of K_2CO_3, in an aromatic nucleophilic substitution condition. In this way, **1** was obtained with 31% yield. This result is similar to those previously described for this procedure [42,43]. Alternatively, we evaluated the Ullmann C−N coupling between 2-bromobenzaldehyde and pyrazole. We applied a ligand-free system composed by CuI and K_3PO_4 in DMF and obtained the target intermediate with an improved yield of 53%. It is important to mention that carbonyl protection was not

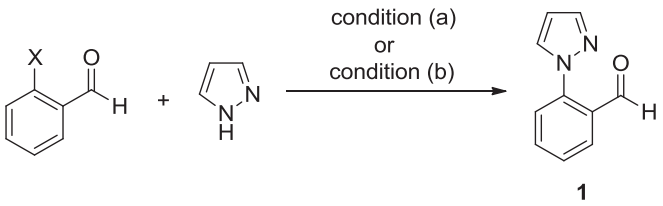

1

condition (a): X = F, K_2CO_3, DMF 110 °C, 24h (31% yield)
condition (b): X = Br, CuI, K_3PO_4, DMF, 75 °C, 24h (53% yield)

Scheme 1. Two strategies employed in the synthesis of the pyrazolylbenzaldehyde **1**.

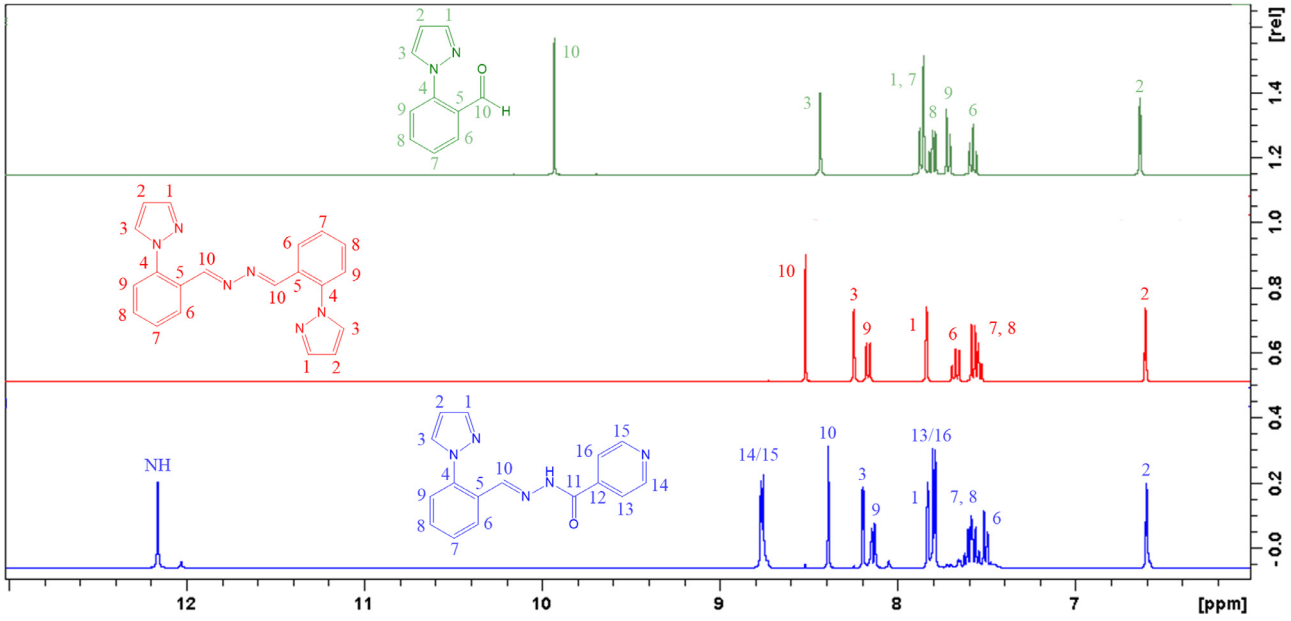

Fig. 1. ^{1}H NMR (400 MHz) spectra of compounds **1** (green), **2** (red) and **3** (blue) in DMSO–d_6 at room temperature.

necessary and that this is the first report of an Ullmann reaction between these chemicals. Thus, this methodology afforded the desired compound with superior results in comparison to the experimental methods published formerly.

Aldehyde **1** was initially prepared in order to expand the chemical diversity in our compound library of moderate metal-binding *N*-acylhydrazones. However, when reacting this product with isoniazid in strong acidic medium, under reflux, single crystals of the dihydrazone **2** {1,2-bis[2-(1H-*pyrazol*-1-*yl*)*benzylidene*]hydrazone} were unexpectedly isolated as the reaction's main product. Isoniazid is an anti-tuberculosis drug widely employed as an important construction block in the Schiff-base condensation synthesis of isonicotinoyl hydrazones.

On the other hand, when performed in milder conditions, this reaction afforded single crystals of the intended *N*-acylhydrazone **3** [2-(1H-pyrazol-1-yl)benzaldehyde isonicotinoyl hydrazone]. Our proposition is that the isonicotinoyl hydrazone may actually be formed at first, since imine generation usually occurs immediately upon the mixture of the reactants, specially under acidic catalysis. However, further protonation on the carbonyl group increases the carbon's electrophilicity, making it susceptible to a nucleophilic attack by a solvent molecule (i.e., ethanol). The subsequent intramolecular electron rearrangement results in breaking of the N–C bond, thus producing a terminal hydrazone derived from the structure of aldehyde **1**. Since free **1** is still present in the reaction mixture, a new C=N bond is formed, yielding the dihydrazone **2**.

In order to obtain the originally desired hydrazone **3**, the synthesis was repeated at room temperature and under less acidic conditions. Additionally, compound **2** was also obtained from the reaction between two equivalents of **1** and one of hydrazine.

Fig. 1 displays the ^{1}H NMR spectra (DMSO–d_6) of pyrazolylbenzaldehyde (**1**) and its derived compounds **2** and **3**. The aldehyde, characterized through its typical de-shielded hydrogen (H10) at 9.93 ppm, is clearly converted into azomethines, observed at 8.52 ppm in **2** and 8.39 ppm in **3**. In the latter, a characteristic aroylhydrazone NH singlet appears at 12.16 ppm, in accordance to previously published isonicotinoyl hydrazones [19,20]. All the signals in the ^{13}C NMR spectra, as well as those related to aromatic hydrogens have been unequivocally assigned using 2D-NMR experiments COZY, HSQC and HMBC (Supplementary Information, Figures S1–10). H2, the most shielded hydrogen, displays a triplet signal at around 6.60 ppm observable in the spectra of all three compounds. The equivalent hydrogens of the pyridinic ring derived from isoniazid, on the other hand, can be detected as a pair of doublets of doublets at 8.76 and 7.80 ppm in compound **3**, also in accordance with our previous studies. They are obviously absent in the spectrum of **2**. Tables S1, S2 and S3 present a thorough report of all the chemical shifts and couplings for ^{1}H and ^{13}C NMR of compounds **1, 2** and **3**.

The aldehyde-derived compounds belonging to system I were isolated as single crystals suitable for X-ray diffraction studies, which allowed for their complete solid-state characterization. The crystal structure investigations of compounds **2** and **3** indicate that both crystallize in the monoclinic system, although in different space groups: $P2_1/c$ and $P2/c$, respectively, containing four molecules per unit cell. Fig. 2 exhibits the molecular representation of the crystal structures and the crystallographic details for these compounds are listed in Table 1. Apart from the characteristic aroylhydrazone NH in **3**, no protonation, counter-ions or solvent molecules are observed in either structures. The lack of solvent molecules in the crystal networks of **2** and **3** is confirmed by the thermal decomposition patterns of both compounds (data not shown), with no mass loss below 200 °C. The solution NMR spectra also show no additional protonation. As expected, the *E* configuration is predominant around the C=N bonds, due to its greater stability.

Selected geometrical parameters for these compounds are displayed in Table 2.

In the solid-state, the molecule of the dihydrazone **2** is not symmetric as one would expect, and the main difference between each phenyl-pyrazole fragment is in the torsion angles amid the planes defined by N1(a), N2(a), C1(a), C2(a) and C3(a) - pyrazole ring - and C4(a), C5(a), C6(a), C7(a), C8(a) and C9(a) - phenyl ring. In one fragment, the angle is equal to 51.5° and, in the other, to 53.7° The phenyl rings from each fragment are also not in the same plane, displaying a dihedral angle of 9.3° The C=N–N=C link between the fragments, showing average C=N distances of 1.272(2) Å, present a torsion angle of 176.1° The crystal stability is guaranteed by non-conventional CH···N hydrogen bond interactions between the pyrazole rings of two dihydrazone molecules, giving rise to a dimeric arrangement. A number of these dimers, on the other hand, are linked by CH···π interac-

Table 1
Crystal data and refinement parameters for compounds **2** and **3**.

	Compound **2**	Compound **3**
Formula	$C_{20}H_{16}N_6$	$C_{16}H_{13}N_5O$
Formula weight (g mol^{-1})	340.39	291.31
Crystal system, space group	Monoclinic, $P2_1/c$	Monoclinic, P2/c
Temperature (K)	293	293
a (Å)	7.9805(5)	12.3523(6)
b (Å)	22.589(1)	7.9564(4)
c (Å)	10.3283(5)	15.3018(8)
β (°)	107.618(6)	96.325(5)
V (Å^3)	1774.5(2)	1494.7(1)
Z	4	4
Radiation type	Mo K*α*	Mo K*α*
μ (mm^{-1})	0.081	0.086
Crystal size (mm)	0.90 × 0.38 × 0.20	0.26 × 0.20 × 0.14
Measured / Independent reflections	37,675/4752	38,444/4054
Observed reflections / R_{int}	2963/0.0491	3187/0.0304
Number of parameters	238	200
R_{obs}, R_{all}	0.0540, 0.0909	0.0505, 0.0654
wR_{abs}, wR_{all}, S	0.1429, 0.1667, 1.063	0.1378, 0.1460, 1.081
Δ*ρ*max, Δ*ρ*min (e Å^{-3})	0.157, −0.154	0.227, −0.173

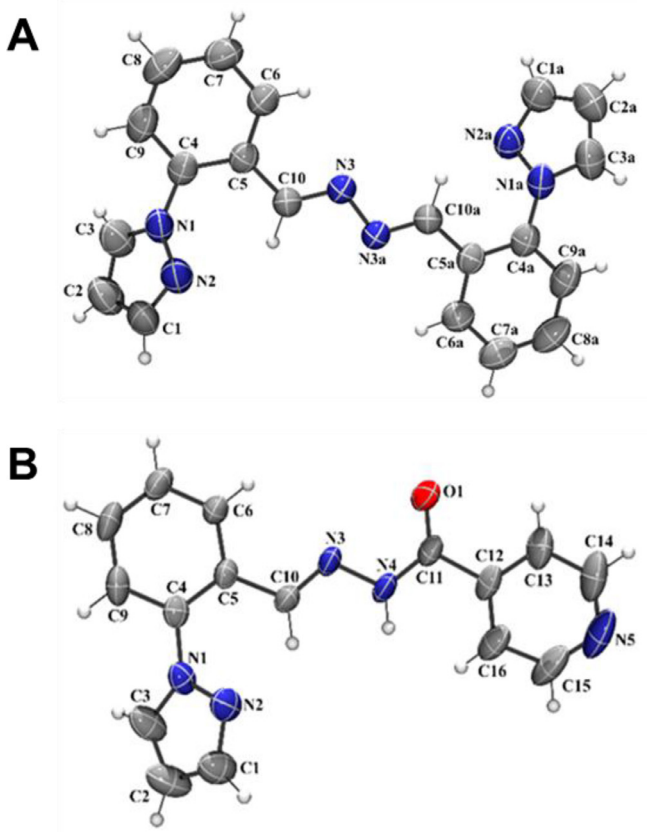

Fig. 2. Crystal structure representations of **(A)** compound **2** and **(B)** compound **3**. The ellipsoids were drawn at the 50% probability level.

Table 2
Selected bond distances and angles for compounds **2** and **3**.

	Compound 2	Compound 3
Bond distances (Å)		
N1−N2	1.359(2)	1.357(2)
N3−N3a / N3−N4	1.407(2)	1.375(1)
N1a−N2a	1.361(2)	–
C10−N3	1.273(2)	1.267(2)
C10a−N3a / C11−N4	1.270(2)	1.348(2)
C11−O1	–	1.211(2)
Bond angles (°)		
C4−N1−N2	121.7(1)	121.5(1)
C5−C4−N1	118.0(2)	96.03(1)
C4−C5−C10	123.1(1)	121.5(1)
C5−C10−N3	119.8(1)	119.2(1)
C10−N3−N3a / C10−N3−N4	112.9(1)	115.9(1)
N3−N3a−Cl0a / N3−N4−C11	111.4(1)	118.4(1)
N3a−C10a−C5a / N4−C11−C12	121.5(1)	115.4(1)
C4a−N1a−N2a	121.1(1)	–
C5a−C4a−N1a	121.1(1)	–
C4a−C5a−C10a	121.6(1)	–
O1−C11−C12	–	120.6(1)
N4−C11−O1	–	123.9(1)

Intermolecular interactions

D-H···A	**D-H (Å)**	**H···A (Å)**	**D···A (Å)**	**D-H···A (°)**
Compound 2				
C3a-H3a···N2^{i}	0.93	2.46	3.378(2)	170.0
C8-H8···*π* (pyraz.)^{ii}	0.93	3.16	4.031(2)	157.0
Compound 3				
N4-H4···N2^{i}	0.89	2.12	3.005(2)	177.0
C7-H7···O1^{ii}	0.93	2.43	3.194(2)	140.0
C9-H9···N5^{iii}	0.93	2.52	3.426(2)	166.0
C3-H3···N3^{iv}	0.93	2.74	3.494(2)	138.0

Symmetry codes: **2** - *i* (1 - *x*, -*y*, -*z*); *ii* (1 + *x*, *y*, *z*).
3 - *i* (-*x*, *y*, ½ - *z*); *ii* (-*x*, 2 - *y*, -*z*); *iii* (*x* - 1, 1 - *y*, *z* - ½); *iv* (-*x*, 1 - *y*, -*z*).

tions involving phenyl and pyrazole rings, respectively, which generates a one-dimensional network along the crystallographic axis ***a*** (Fig. 3A).

Concerning compound **3**, the torsion angles between aromatic rings are 28.1° (phenyl-pyridyl) and 47.4° (phenyl-pyrazole). In this case, the carbon-nitrogen distances in the CNNC group are different [1.267(2) and 1.348(2) Å], which indicates that one linkage has double bond character while the other is a single bond. For this reason, N4 is protonated, contrary to what is observed in compound **2**. It is precisely the occurrence of the hydrazonic N4H group which stabilizes the crystal structure of **3**, acting as a hydrogen donor in weak NH···N hydrogen bonds involving pyrazole N2 atoms as the acceptors. These interactions generate, as was also observed in the structure of **2**, dimers. Non-conventional CH···O and CH···N contacts involving the heteroatoms O1, N5 and N3 link the dimers, giving rise to a more complex tri-dimensional network (Fig. 3B).

The Hirshfeld surface (HS) analysis [44] of the compounds (Fig. 4A) indicates that the most important interaction is CH···N in **2** and NH···N in **3**. Comparing the HS of both derivatives, it is

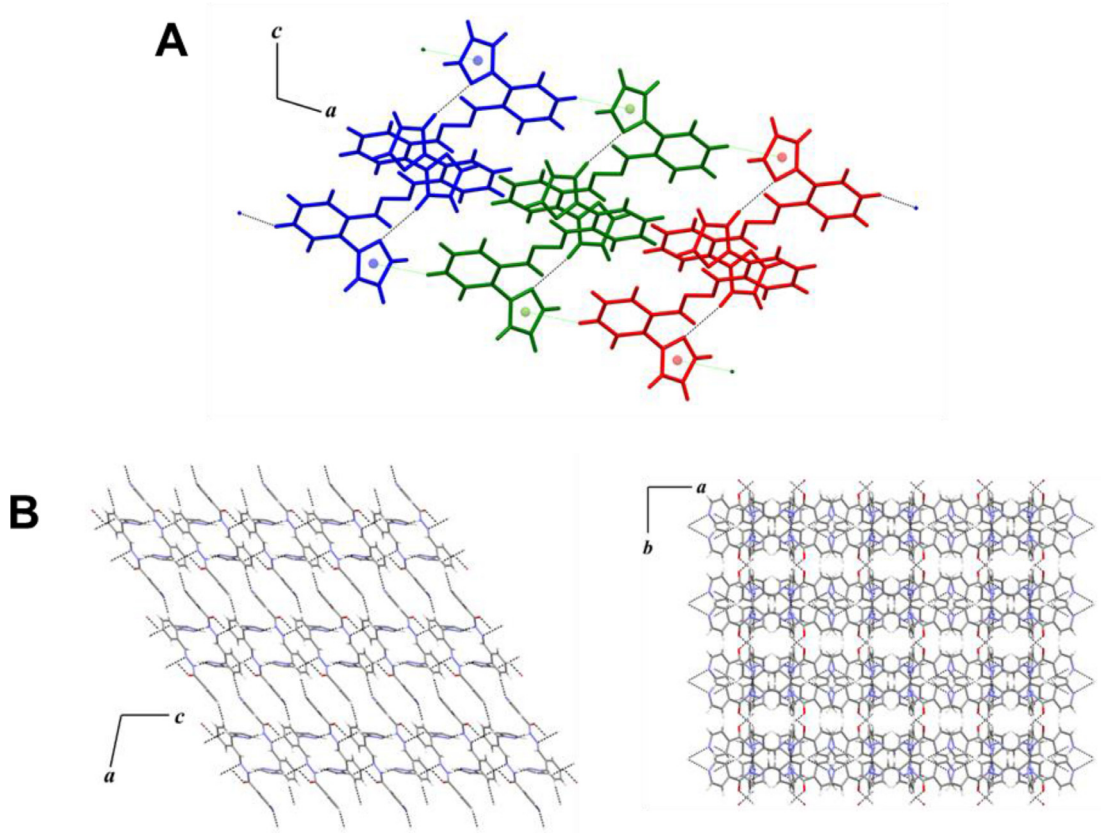

Fig. 3. Intermolecular interactions in **(A)** compound **2**, where each color represents a dimeric unit linked in a one-dimensional network along the crystallographic axis ***a*** and **(B)** compound **3**. The intricate tridimensional network can be observed along axis ***b*** (left) and ***c*** (right).

possible to perceive the difference in their shapes and volumes (434.94 Å^3 for **2** and 365.71 Å^3 for **3**), as expected. The fingerprint plot analysis [45] show that the distribution of intermolecular interactions is also unlike in both compounds, as can be seen in Fig. 4B. The most representative interaction in these solids are the nondirectional H···H contacts, that represent 50.4% and 42.2% for **2** and **3**, respectively (Figure S11). In both compounds, the N···H contacts related to CH···N and NH···N hydrogen bonds are the most relevant interactions in the crystal structures [*di* + *de* equal to 2.3 in **2** (Figure S11A) and 2.0 in **3** (Figure S11B)], and these contacts have similar contribution in both compounds (14.6% in **2** and 17.8% in **3**). For the aroylhydrazone **3**, the observed O···H interaction corresponds to a contribution of 9.5% (Figure S11B).

The analysis of energy frameworks [46] for these compounds indicates that in **2** the strongest interactions are related to CH···N (−66.7 kJ mol^{-1}), the stacking arrangement along the [02–1] direction (−67.0 kJ mol^{-1}) and CH···π (−29.1 kJ mol^{-1}), in which the dispersion energy contribution is more important than the electrostatic energy for the total energy frameworks (Figure S12A). On the other hand, the strongest interaction in **3** is the hydrogen bond NH···N (−105.0 kJ mol^{-1}), which contributes with the highest electrostatic energy for the total (Figure S12B). The energy frameworks representations for the total interaction energy of dihydrazone **2** and aroylhydrazone **3** can be observed in Fig. 5. As expected, the intermolecular interactions show anisotropic 3D topology for both compounds. In **2**, the strongest interactions, which include CH···N and CH···π contacts, occur in the [101] direction (Figure S13A) and the weakest interactions are observed in the [010] direction. In this compound, the dispersion contribution is more relevant for the crystal packing. On the other hand, in the crystal of compound **3**, the strongest interactions, representing the NH···N hydrogen bonds, are observed in the [010] direction and the weakest ones, including non-conventional hydrogen bonds like CH···N, are in the [100] direction (Fig. 5B). The energy framework (Figure S13B) shows that, in the aroylhydrazone, both the electrostatic and the dispersive contributions are important for crystal packing, mostly depending on the crystallographic direction considered, being the electrostatic one more relevant along [010] and the dispersion energy in the direction [100].

The gas phase structures of compounds **2** and **3** were optimized at the CAM-B3LYP/6–311+*G*(2d,p) level of theory and are in excellent agreement with the X-ray measurements, presenting root-mean-square deviation (RMSD) values of 0.3365 and 0.1852 Å, respectively. Fig. 6 shows the overlapping of the optimized gas phase structures and those obtained from the crystallographic analyses, shown in yellow.

The mid-infrared (IR) spectra of the aldehyde precursor **1** (Figure S14A) and its derivatives **2** and **3** (Figure S14B and C, respectively) confirm some of the structural aspects observed in the crystal structures of the latter two compounds. The spectrum of **1** shows the well-known aldehyde ν(C–H) absorptions at 2880 and 2765 cm^{-1}. These modes, however, are completely absent in the spectra of products **2** and **3**. Likewise, the lack of the aldehyde ν(C=O) band at 1685 cm^{-1} was observed in the spectrum of **2**. However, it cannot be confirmed for aroylhydrazone **3**, since this compound presents intense carbonyl coupled modes [ν(C=O) + β(H–N–C)] in the region. Another important vibrational mode observed in **3** but not in **2** is the distinguishing ν(N–H) absorption at 3185 cm^{-1}. On the other hand, coupled azomethine modes can be found in the spectra of both hydrazones, at 1619 [ν_{as}(C=N) + β(H–C=N)] for **2** and 1640

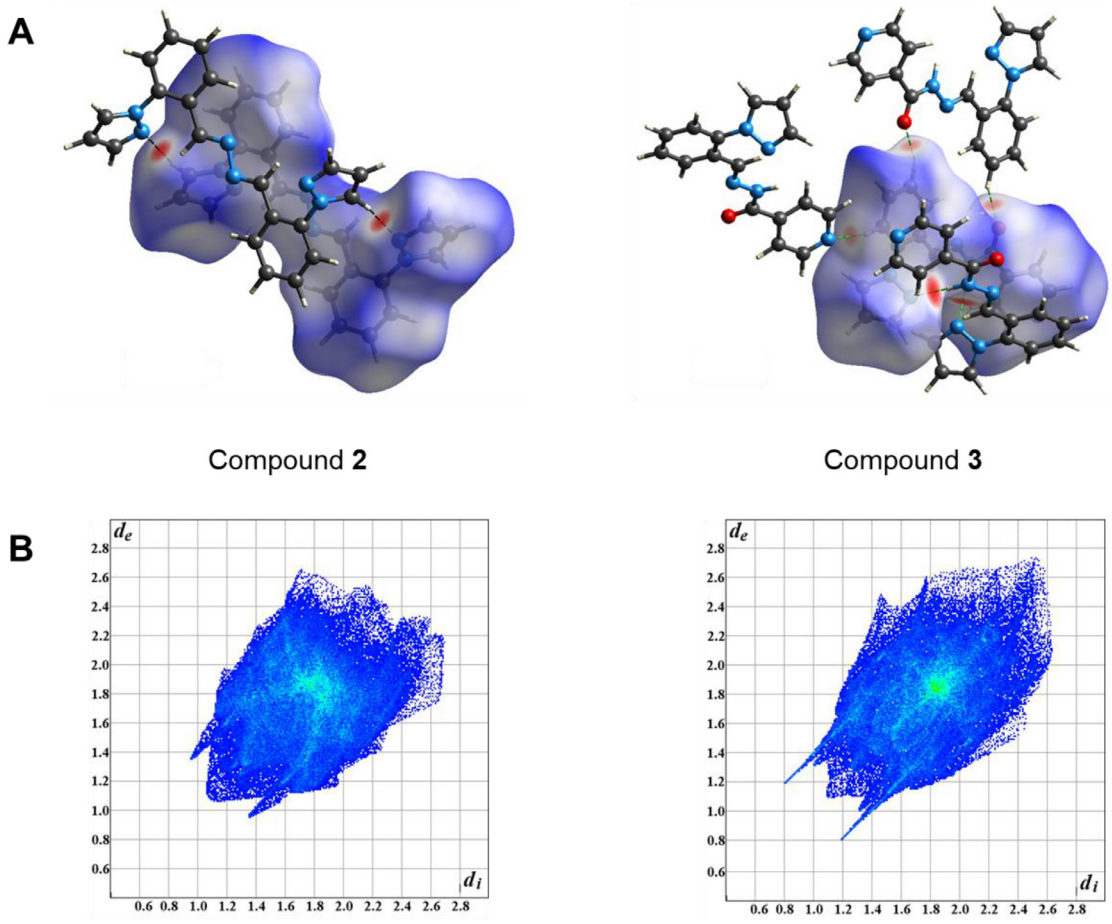

Fig. 4. **(A)** Hirshfeld surfaces and **(B)** fingerprint plots for compounds **2** and **3**.

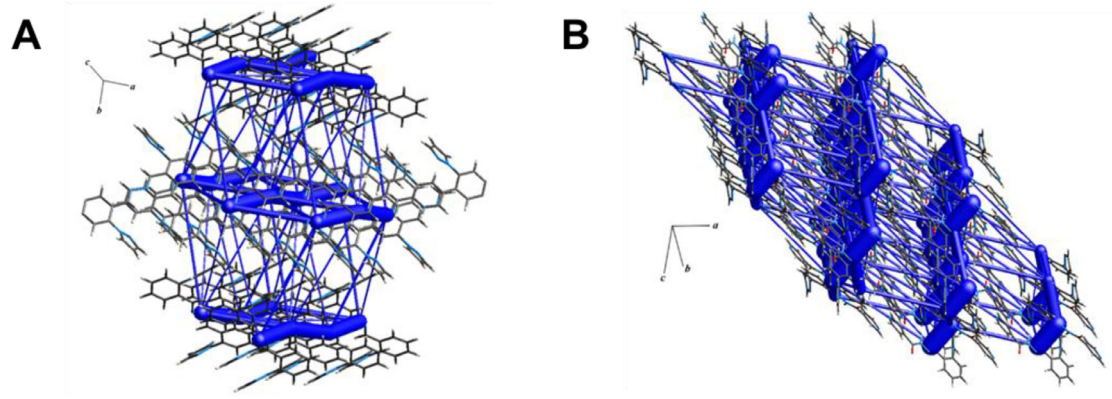

Fig. 5. Energy framework diagrams for the total interaction energy of **(A)** compound **2** and **(B)** compound **3**. All diagrams were prepared using cylinder scale of 100.

[ν(C=N) + β(H−C=N)]/1562 [β(H−N−N) + β(H−C=N)] cm^{-1} for the aroylhydrazone **3**. These absorptions are in accordance with our previously published isonicotinoyl hydrazones [12, 13, 19]. Characteristic pyrazole bands were assigned at 1394 (**2**)/1397 (**3**) cm^{-1} [ν(N−N)] and at 767 (**2**) / 768 (**3**) cm^{-1} [γ(H−C)]. The main experimental IR absorptions for hydrazones **2** and **3** are summarized in Table 3, along with the calculated CAM-B3LYP/6–311+*G*(2d,p) vibrations. In general, the calculated frequencies are in accordance with the observed ones. Higher deviations (e.g., the N−H stretching in **3**) may be related to groups involved in hydrogen bonds in the solid-state, as shown by the X-ray structures. The effects of intermolecular interactions are obviously neglected in gas phase calculations.

3.2. 2-(4-metoxyphenoxy)benzaldehyde-derived compounds (system II)

For the synthesis of the second aldehyde, **4** [2-(4-metoxyphenoxy)benzaldehyde], a copper-free protocol based on nucleophilic aromatic substitution on a fluoroarene was applied. Thus, 2-fluorobenzaldehyde and 4-methoxyphenol were reacted in presence of K_2CO_3 and using DMF as solvent (Scheme 2). Compound **4** was isolated in 71% yield.

The isonicotinoyl hydrazone derivative of aldehyde **4**, compound **6**, was initially proposed as a tridentate ligand for the binding of physiological metal ions, which would count with the benzoether oxygen, the azomethine nitrogen and the carbonyl oxy-

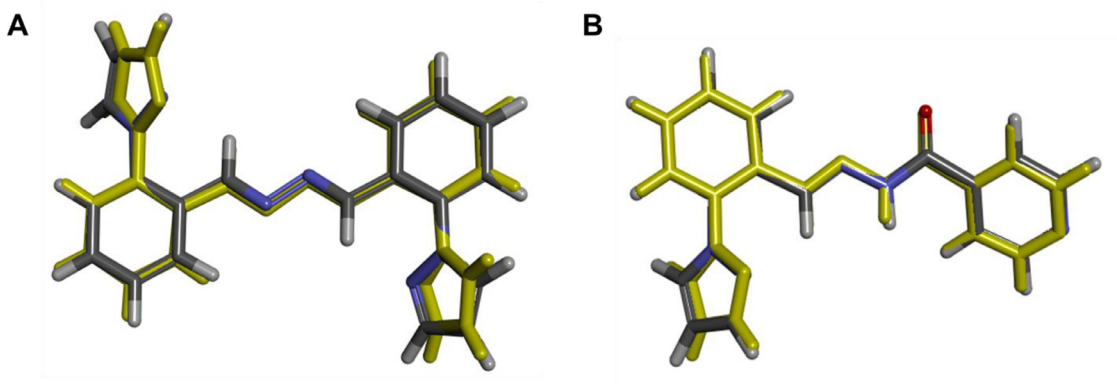

Fig. 6. Overlap of DFT optimized and X-ray (yellow) structures for compounds **(A) 2** and **(B) 3**.

Table 3
Assignment of the main IR absorptions of compounds **2** (scale factor: 0.985, $R^2 = 0.9973$) and **3** (scale factor: 0.956, $R^2 = 0.9975$).

Compound 2				Compound 3				Assignments
Experimental	Calculated			Experimental	Calculated			
	Unscaled	Scaled	IR intensity		Unscaled	Scaled	IR intensity	
–	–	–	–	3185	3558.6	3402.0	11.30	ν(N–H)
–	–	–	–	3062	3120.1	2982.8	27.14	ν(C–H)$_{azomethine}$
–	–	–	–	1686	1798.6	1719.5	314.7	ν(C=O) + β(H–N–C)
–	–	–	–	1640	1727.0	1651.0	6.591	ν(C=N)$_{azomethine}$ + β(H–C=N)$_{azomethine}$
1619	1736.5	1710.5	199.6	–	–	–	–	ν_{as}(C=N)$_{azomethine}$ + β(H–C=N)$_{azomethine}$
–	–	–	–	1562	1578.4	1509.0	375.6	β(H–N–N) + β(H–C=N)$_{azomethine}$
–	–	–	–	1556	1547.0	1478.9	53.77	ν(C=C)$_{pyridine}$ + β(H–C=C)$_{pyridine}$
1394	1342.2	1322.1	10.89	1397	1344.8	1285.6	7.217	ν(N–N)$_{pyrazole}$ + β(H–C=C)$_{benzene}$
–	–	–	–	1282	1263.3	1207.7	64.64	ν_{as}(C=N)$_{pyridine}$ + ν_{as}(C=C)$_{pyridine}$
–	–	–	–	1148	1192.2	1139.7	174.1	ν(N–N)$_{hydrazone}$
1049	1008.1	993.0	13.13	1055	999.6	955.6	5.026	γ(H–C)$_{azomethine}$ + γ(H–C)$_{benzene}$
767	768.7	757.2	110.0	768	771.8	737.8	74.39	γ(H–C)$_{pyrazole}$
–	–	–	–	682	704.9	673.9	44.17	ν_{sym}(C=N)$_{pyridine}$

ν: stretching; β: in-plane bending; γ: out-of-plane bending; as: asymmetric; *sym*: symmetric.

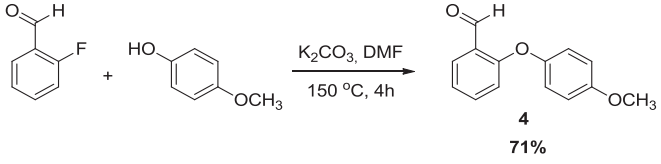

Scheme 2. Synthesis of 2-(4-metoxyphenoxy)benzaldehyde **4**.

gen as donor atoms. As observed in the previous system, however, reaction of **4** with isoniazid in strong acidic medium and under reflux afforded dihydrazone **5** instead of the desired product. On the other hand, reaction between aldehyde **4** and isoniazid in mild conditions resulted in the isonicotinoyl hydrazone **6**. For the purposes of this study, compound **5** was also obtained in higher yields by reacting **4** with hydrazine in a 2:1 stoichiometry.

The ^{1}H NMR spectra (DMSO–d_6) of the three compounds constituting system II are displayed in Fig. 7. Inhere, as opposed to system I, little change is observed in the aromatic hydrogen atoms when comparing the spectra. On the other hand, the shielding observed for H7 is due to the change in its chemical environment, going from aldehyde in **4** (10.44 ppm) to azomethines in **5** and **6** (8.96 and 8.91 ppm, respectively). In the latter compound, the two isoniazid characteristic doublets of doublets are present at 8.89 and 8.06 ppm, and the distinctive hydrazonic NH resonates at 12.32 ppm. The three methoxy hydrogens H14 absorb at 3.77 ppm in **4** and at 3.75 ppm in **5** and **6**. Once again, a detailed report of all the absorptions and observed couplings is summarized in Tables S4, S5 and S6, while ^{13}C and bidimensional spectra are supplied as Figures S15–24.

In the solid-state, thermogravimetric decomposition of compound **5** occurs in one step between around 250 to 350 °C (data not shown), evidencing the absence of solvation molecules in the network. Compound **6**, on the other hand, has a more complex thermal degradation. The presence of one crystallization water molecule in the structure of **6** was proposed based on the loss of 4% of its molecular weight between 100 and 130 °C.

Since no single crystal was obtained during the preparation of the hydrazonic compounds belonging to system II, theoretical gas phase calculations were performed to shed light into some structural aspects of **5** and **6**. The same approach previously used for optimizing compounds **2** and **3** was employed, because good agreement was found between the calculated and crystallographic data. Based on NMR experiments performed between 25 and 65 °C (Figure S25), no isomerization or conformational changes seem to occur in the structures of aroylhydrazones **3** and **6**, in the range of temperatures evaluated. The only alterations observed in the spectra are related to the expected displacements due to the increase in temperature (insets in Figure S25A and B). For this reason, and because of the similarity between systems I and II, the herein optimized structures were calculated for the *E* isomers for both dihydrazone **5** and aroylhydrazone **6** (Fig. 8). In the latter, an *anti* conformation was assumed as well. Selected calculated bond distances and angles are shown in Table 4.

Confirming the suitability of the computational approach chosen in the absence of crystal structures, characteristic dihydrazone and aroylhydrazone theoretical bond distances and angles are very similar to those obtained both experimentally (X-ray diffraction) and by DFT calculations for the related compounds **2** and

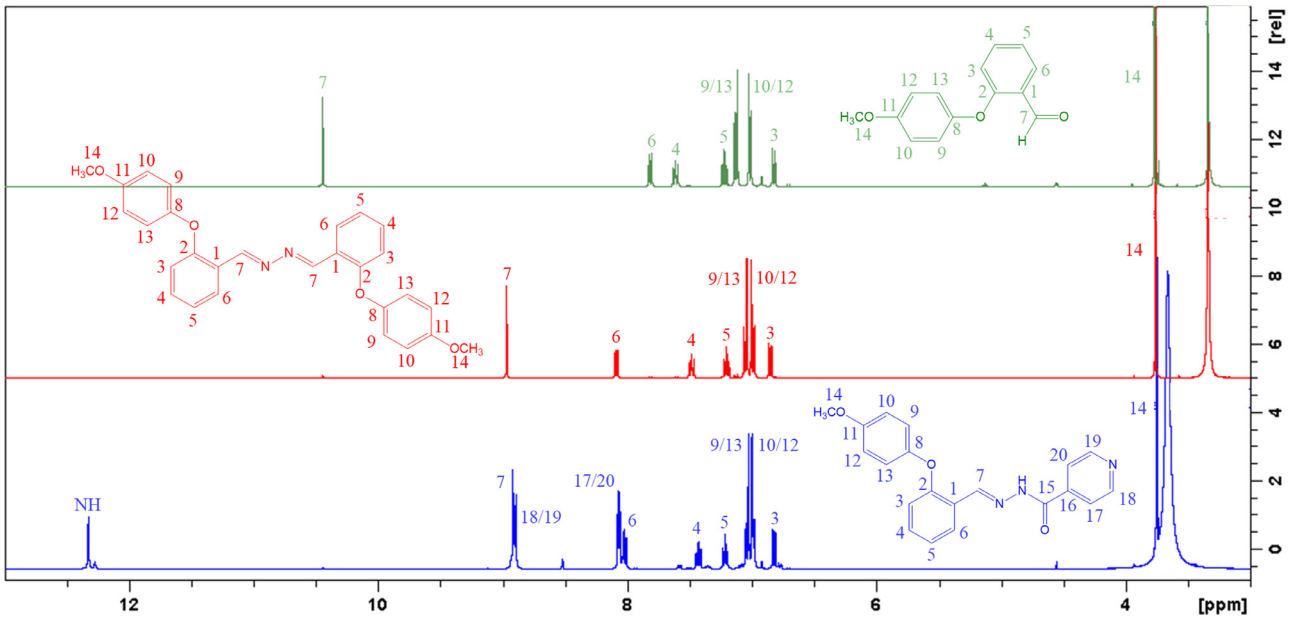

Fig. 7. ^{1}H NMR spectra (400 MHz) of compounds **4** (green), **5** (red) and **6** (blue) in DMSO–d_6 at room temperature.

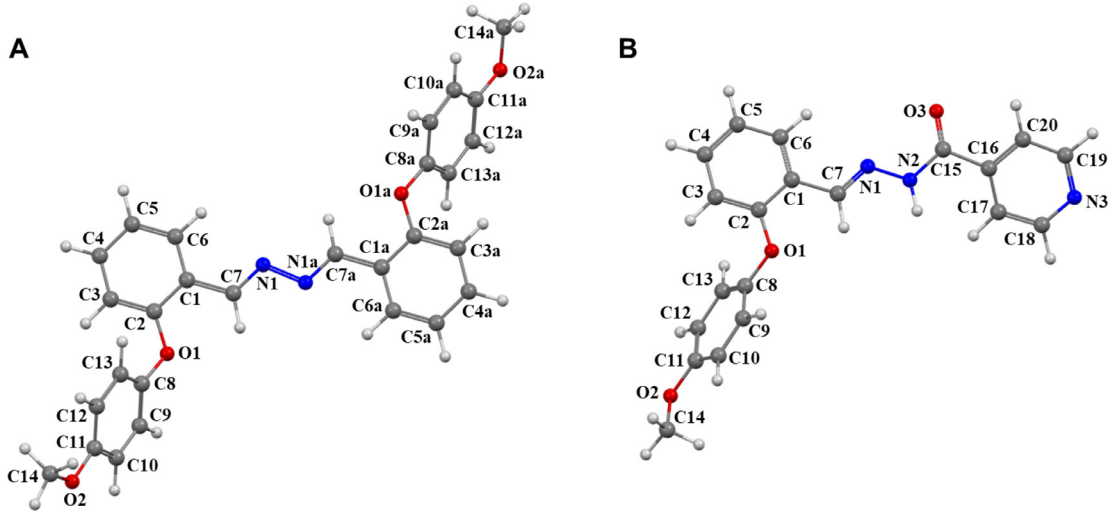

Fig. 8. Gas phase optimized structures of **(A)** compound **5** and **(B)** compound **6**.

Table 4
Selected calculated HF-3c bond distances and angles for compounds **5** and **6**.

	Compound 5	Compound 6
Bond distances (Å)		
C2–O1 (C2a–O1a)	1.368	1.370
O1–C8 (O1a–C8a)	1.375	1.375
C7–N1 (C7a–N1a)	1.273	1.269
N1–N1a / N1–N2	1.416	1.364
N2–C15	–	1.404
C15–O3	–	1.206
Bond angles (°)		
C8–O1–C2 (C8a–O1a–C2a)	121.0	120.7
O1–C2–C1 (O1a–C2a–C1a)	117.2	117.2
C2–C1–C7 (C2a–C1a–C7a)	119.8	119.6
C1–C7–N1 (C1a–C7a–N1a)	120.0	119.7
C7–N1–N1a (C7a–N1a–N1) / C7–N1–N2	113.1	118.7
N1–N2–C15	–	118.9
N2–C15–C16	–	114.5
N2–C15–O3	–	123.4
O3–C15–C16	–	122.0

3, with the exception of some NH-related parameters between the *N*-acylhydrazones **3** and **6**. Besides this, other observed differences are obviously associated with the aldehyde-derived moieties, which are not the same in systems I and II.

Concerning the differences between **5** and **6**, hydrazonic N–N bond is shorter in the aroylhydrazone, which was also noticed in the data concerning compounds **2** and **3**. Related C=N–N angles, on the other hand, are larger for **3** and **6**, when comparing them to **2** and **5**, respectively. The effects are probably due to the particularities of electron delocalization in aroylhydrazones, in which imine and amide groups are conjugated.

The IR spectra of the compounds belonging to system II can be seen in Figure S26A-C. While the characteristic aldehyde ν(C–H) absorptions occur at 2890 and 2775 cm^{-1} in compound **4**, its ν(C=O) mode can be observed as a band centered at 1685 cm^{-1}. No major inductive effects derived from the substitution of the *ortho*-*N*-pyrazolyl by the *ortho*-4-methoxyphenoxyl group in the benzaldehyde ring were noticed when comparing the –CHO vibrational frequencies of **4** with those of **1**. Such absorptions are

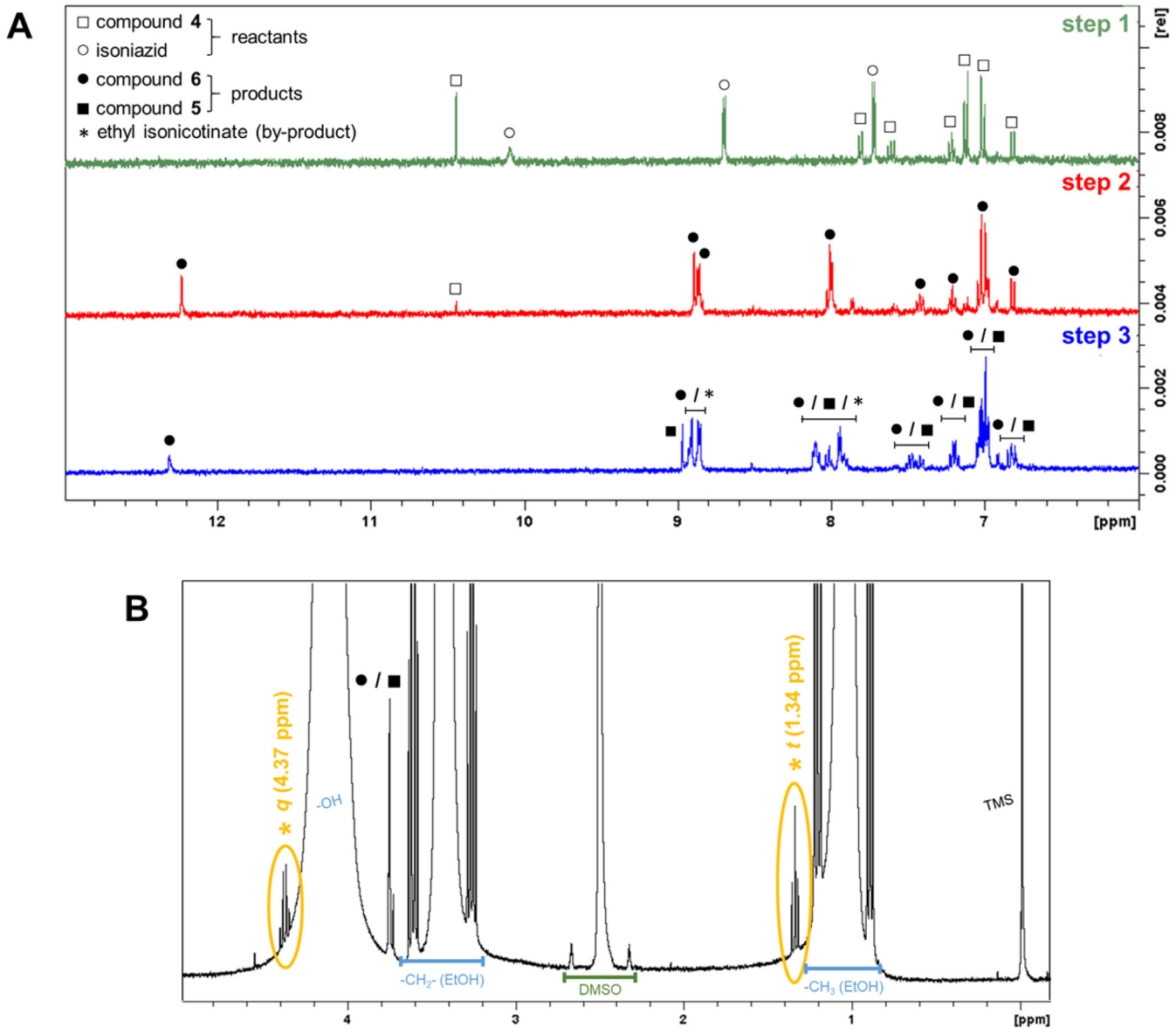

Fig. 9. (A) ^{1}H NMR spectra (400 MHz) of aliquots from different steps in the synthesis of compounds **5**: step 1 (immediately after the dropwise addition of isoniazid to compound **4** – green), step 2 (after the addition of acid catalyst – red) and step 3 (after 3 h of reflux – blue) in DMSO–d_6 at room temperature. **(B)** High-field region of the ^{1}H NMR spectrum from step 3, highlighting in yellow the signals associated with the formation of ethyl isonicotinate as a by-product.

not present in the spectrum of dihydrazone **5**, indicating that the isolated product is aldehyde-free. The azomethine ν_{as}(C=N) mode is, as previously observed for dihydrazone **2**, coupled with in-plane H–C=N bending movements, occurring at 1620 cm^{-1}. Aroylhydrazone **6**, on the other hand, although also aldehyde-free [as confirmed by the absence of ν(C–H) bands at 2890 and 2775 cm^{-1}], possesses a series of complex, overlapped modes in the ν(C=O) region. The main bands associated with this spectral interval are present at 1682 cm^{-1} [ν(C=O) + β(H–N–C)] and 1637 cm^{-1} [ν(C=N)$_{azomethine}$ + β(H–C=N)$_{azomethine}$]. The characteristic *N*-acylhydrazone ν(N–H) absorption can be found at 3175 cm^{-1}. In both compounds, typical methoxyl bands were observed at 2832 (**5**) / 2833 (**6**) cm^{-1} [ν(C–H)] and at 1038 (**5**) / 1034 (**6**) cm^{-1} [ν_{as}(C–O–C)]. Additionally, asymmetric aromatic C–O–C ether stretching modes, coupled with in-plane bending H–C=C vibrations of the *ortho*-4-methoxyphenoxyl moiety, were assigned at 1230 and 1234 cm^{-1} for compounds **5** and **6**, respectively, with the aid of computational tools. The main experimental IR absorptions for hydrazones **5** and **6** are summarized in Table 5, along with the calculated CAM-B3LYP/6–311+*G*(2d,p) vibrations. Once again, theoretical frequencies are, as a whole, in good agreement with the observed ones.

Additional ^{1}H NMR experiments were performed in system II to support the mechanistic proposition for the observed unexpected formation of the dihydrazones. The dropwise addition of isoniazid to **4**, both in ethanol, produces neither change of color nor precipitation. On the other hand, addition of 3 drops of conc. hydrochloric acid as catalyst immediately turns the solution bright yellow and some precipitation can be noticed. When reflux begins, the precipitate is redissolved. Aliquots from the reaction mixture were taken at three different moments, namely: step 1 (immediately after the mixture of both reagents), step 2 (after the addition of catalyst) and step 3 (after a 3-hour reflux). The corresponding ^{1}H NMR spectra, in the 13.0–6.0 ppm range, are displayed in Fig. 9A.

Interestingly, the spectrum related to step 1 (green) shows that no reaction occurs at room temperature upon mixture of **4** and

Table 5
Assignment of the main IR absorptions of compounds **5** (scale factor: 0.951, R^2 = 0.9994) and **6** (scale factor: 0.951, R^2 = 0.9981).

Compound 5				Compound 6				Assignments
Experimental	Calculated			Experimental	Calculated			
	Unscaled	Scaled	IR intensity		Unscaled	Scaled	IR intensity	
–	–	–	–	3175	3543.9	3370.2	10.5	ν(N–H)
–	–	–	–	3056	3017.8	2869.9	60.6	$\nu(C-H)_{azomethine}$
2832	3026.0	2877.7	53.08	2833	3031.0	2882.5	47.9	$\nu(C-H)_{MeO}$
–	–	–	–	1682	1798.3	1710.2	322.6	ν(C=O) + β(H–N–C)
–	–	–	–	1637	1727.1	1642.5	23.3	$\nu(C=N)_{azomethine}$ + $\beta(H-C=N)_{azomethine}$
1620	1737.2	1652.1	298.6	–	–		–	$\nu_{as}(C=N)_{azomethine}$ + $\beta(H-C=N)_{azomethine}$
–	–	–	–	1555	1576.6	1499.3	403.5	β(H–N–N) + $\beta(H-C=N)_{azomethine}$
1506	1565.4	1488.7	375.5	1508	1567.0	1490.2	274.6	$\beta(H-C=C)_{benzene-MeO}$ + $\beta(H-C=C)_{benzene}$
1502	1545.3	1469.6	536.2	1504	1546.4	1470.6	227.6	
–	–	–	–	1371	1422.2	1352.5	55.1	$\beta(H-C-C)_{azomethine}$ + β(H–N–N)
1230	1278.3	1215.7	995.2	1234	1284.2	1221.3	471.1	$\nu_{as}(C-O-C)_{aromatic\ ether}$ + $\beta(H-C=C)_{benzene-MeO}$
–	–	–	–	1148	1183.6	1125.6	135.3	$\nu(N-N)_{hydrazone}$
1038	1072.0	1019.5	126.2	1034	1092.8	1039.3	56.4	$\nu_{as}(C-O-C)_{MeO}$
961	931.8	886.1	29.1	964	918.3	873.3	22.2	$\nu_{sym}(C=C)_{benzene-MeO}$ + $\beta(C=C-C)_{benzene}$
762	777.5	739.4	109.4	765	775.1	737.1	48.0	$\gamma(H-C)_{benzene}$
–	–	–	–	686	704.7	670.2	62.3	$\nu_{sym}(C=N)_{pyridine}$

ν: stretching; β: in-plane bending; γ: out-of-plane bending; as: asymmetric; *sym*: symmetric.

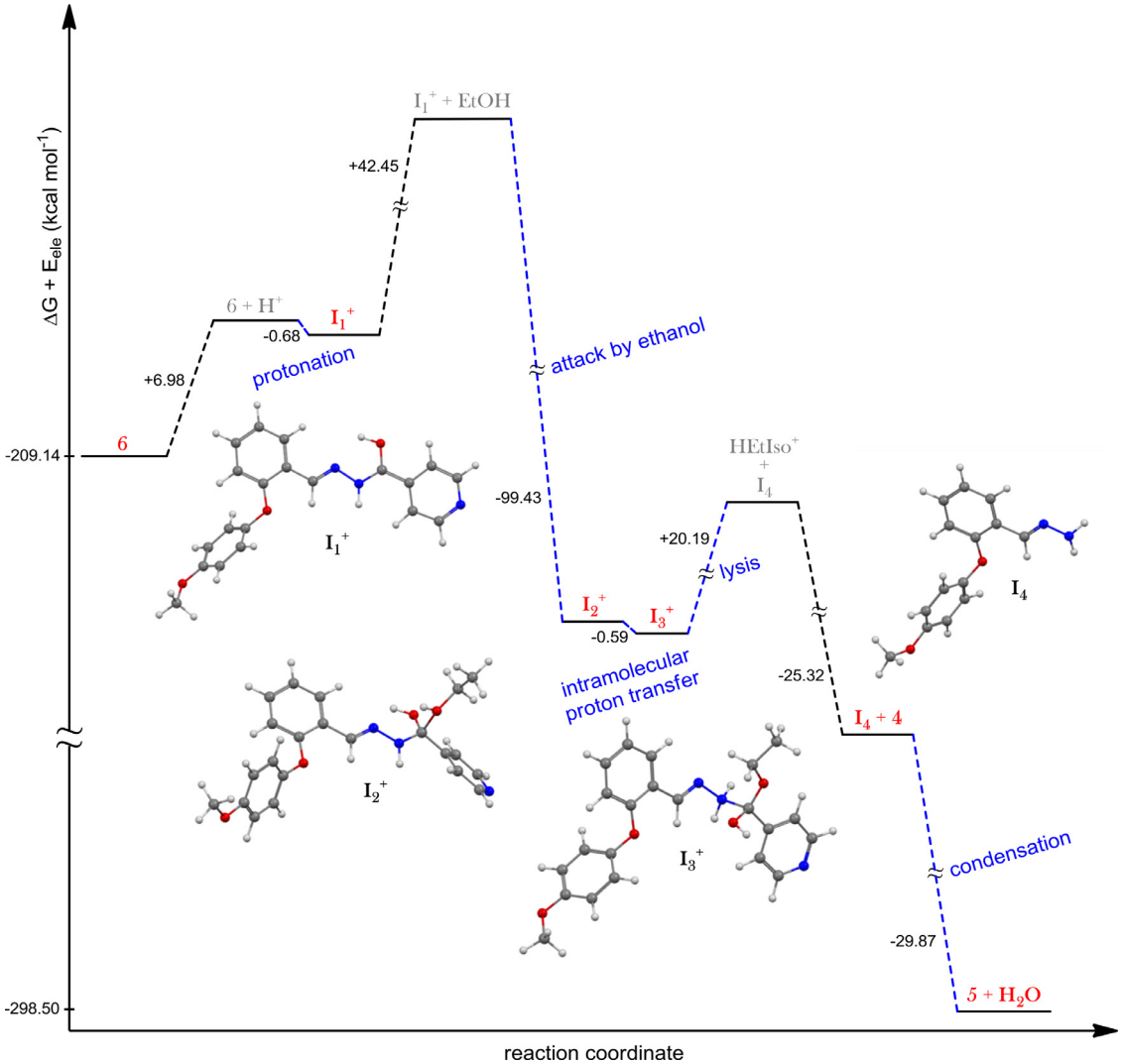

Fig. 10. Calculated HF-3c energetic profile (ΔG + electronic energy) for the conversion of **6** into **5**. The most important steps are labelled in blue. Reaction intermediates $\mathbf{I_1}^+$, $\mathbf{I_2}^+$, $\mathbf{I_3}^+$ and $\mathbf{I_4}$ are highlighted in red color and their gas phase optimized structures are also shown.

isoniazid in the absence of catalyst, and the signals referring to the unmodified aldehyde and isonicotinic acid hydrazide are observed. The absence of any azomethine-associated resonance, together with the presence of the characteristic aldehyde H7 (doublet at 10.44 ppm) and isoniazid's −NH− and $-NH_2$ [10.09 and 4.61 ppm (not shown), respectively] signals are proof of that. After the addition of catalytic amounts of conc. hydrochloric acid (red spectrum), however, a typical imine −HC=N− hydrogen at 8.89 ppm and the distinctive hydrazonic −NH− absorption at 12.23 ppm arise, although some aldehyde is still present in solution. There is great similarity between this spectrum and that of compound **6**, indicating that the hydrazone is formed immediately upon addition of the catalyst. When heating is kept for 3 h, a new equilibrium can be observed (blue spectrum). While some of the isonicotinoyl hydrazone is still present in solution, a new azomethine signal is observed at 8.97 ppm, in accordance with the chemical shift observed for compound **5**-related −HC=N− hydrogen. Moreover, all the resonances of this dihydrazone can be identified in the spectrum as well, indicating the presence of a mixture of derivatives **5** and **6**. The simultaneous occurrence of a quartet at 4.37 ppm and a triplet at 1.34 ppm (Fig. 9B) indicates the formation of ethyl isonicotinate, which is consistent with the expected by-product resulting from the attack on the aroylhydrazone's carbonyl by ethanol, depicting thus a classic solvolysis reaction, followed by condensation of the ensuing hydrazone to a second free aldehyde molecule. Scheme S1 summarizes this proposed reaction pathway for dihydrazone formation, which can probably be also extended to system I since this process does not seem to be aldehyde-dependent and might be related to the presence of isoniazid as a reactant. Nevertheless, a dihydrazone derived from 2-pyridinecarboxaldehyde was isolated in our laboratory as an unexpected solvolysis product from the corresponding *p*-toluenesulfonyl hydrazone (personal communication), which indicates a perhaps broader scope for this pathway.

Insights into the thermodynamics of the conversion **6** → **5** were obtained through a computational approach. Structures of all the reactants and reaction intermediates were optimized in the gas phase and had their individual thermodynamic parameters calculated. Fig. 10 displays the energetic profile (ΔG + electronic energy) for each of the main steps that comprise the process, along with the structures of key-intermediates.

Of the main steps involved in the proposed pathway, only the lysis of intermediate $\mathbf{I_3}^+$ into $\mathbf{I_4}$ and the by-product $HEtIso^+$ (protonated ethyl isonicotinate, whose signals were unequivocally identified in the ^1H NMR spectrum shown in Fig. 9B) is, as expected, endergonic (+20.19 kcal mol^{-1}). Amongst the exergonic steps, the most favorable are the attack by ethanol on the protonated carbonyl of intermediate $\mathbf{I_1}^+$ (–99.43 kcal mol^{-1}) and the condensation between $\mathbf{I_4}$ and a second unit of aldehyde **4** (–29.87 kcal mol^{-1}), to afford the final product **5** and a water molecule.

The global reaction can be represented by the equation:

$$6(\text{aroylhydrazone}) + \text{EtOH} + 4(\text{free aldehyde}) \rightarrow 5(\text{dihydrazone}) + \text{EtIso} + H_2O$$

The process is slightly exergonic as a whole and, therefore, spontaneous, with a calculated ΔG of −1.686 kcal mol^{-1} (−7.054 kJ mol^{-1}) at 298 K. Although this value is rather small, it is important to consider that calculations were performed in the gas phase. Hence, from a strictly thermodynamic point of view, the proposed reaction pathway is quite reasonable. A complete theoretical study employing higher levels of calculation and including solvent effects is underway and will be the subject of a specific future report.

4. Conclusions

Aroylhydrazones are versatile compounds with a series of applications, from biological to technological spheres. The simplicity of their preparation allows for a great chemical variability and synthetic manageability. However, the process can be not as straightforward as one would imagine. Some parameters such as specific reactants, the amount of acid employed as catalyst and reaction temperature can have a direct impact on the obtained product. In the present work, the solvolysis of the initially formed isonicotinoyl hydrazones, leading to two novel dihydrazones, is described.

The novel approach proposed for the synthesis of precursor 2-(1H-pyrazol-1-yl)benzaldehyde (**1**), involving the Ullmann reaction, provided higher yields than the most common aromatic nucleophilic substitution. Reactivity of this aldehyde towards isoniazid afforded different main products, mostly depending on the synthetic conditions employed: a Schiff-base condensation under mild pH and temperature results in 2-(1H-pyrazol-1-yl)benzaldehyde isonicotinoyl hydrazone (**3**), while the use of a strong acidic medium and reflux promote hydrazone solvolysis to yield the dihydrazone 1,2-bis[2-(1H-*pyrazol*-1-*yl*)*benzylidene*]hydrazone (**2**). This compound was also synthesized through the direct reaction between **1** and hydrazine dihydrochloride. Compounds **2** and **3** were obtained in the form of single crystals and characterized by XRD. In the solid-state, the molecules of both products associate to form dimers, which in turn interact through non-conventional hydrogen bonds to generate 1D and 3D networks, respectively.

A very similar outcome was observed for the related system composed by 2-(4-metoxyphenoxy)benzaldehyde (**4**) and its aroylhydrazone and dihydrazone derivatives. Aldehyde **4** was prepared with a copper-free protocol based on nucleophilic aromatic substitution on a fluoroarene. 1,2-bis[2-(4-*methoxyphenoxy*)*benzylidene*]hydrazone (**5**) was obtained either from the reaction between **4** and isoniazid at very low pH and high temperature, or directly by reacting **4** and hydrazine dihydrochloride. On the other hand, the desired 2-(4-metoxyphenoxy)benzaldehyde isonicotinoyl hydrazone (**6**) was isolated only when mild synthetic conditions were applied. Theoretical calculations suggest that the structures of these products are similar to the corresponding hydrazonic derivatives **2** and **3**. System II was employed to support the mechanistic proposition for the unexpected formation of the dihydrazones in the reaction medium: the solvolysis of the isonicotinoyl hydrazone followed by attack to a second aldehyde molecule, as was suggested from ^1H NMR experiments and supported by thermodynamic calculations. From a theoretical point of view, the process is spontaneous as a whole, with a calculated ΔG of −1.686 kcal mol^{-1} (−7.054 kJ mol^{-1}) at 298 K.

Finally, we believe that the synthetic cases discussed herein, supported by strong structural and spectroscopic evidences, as well as by thermodynamic parameters calculated for system II, can be useful to other chemists dealing with the apparently obvious art of preparing aroylhydrazones for a multitude of applications.

Author contribution

JL planned the syntheses of aldehydes **1** and **4**; CCN synthesized and characterized the precursor aldehydes mentioned before; DSC and BNE synthesized and characterized the hydrazonic compounds **2, 3, 5** and **6** as well as obtained single crystals for **2** and **3**; CHFJ selected the appropriate crystals and collected the X-ray diffrac-

tion data; RD solved the structures of compounds **2** and **3** and performed their Hirshfeld and energy frameworks analyses; LASC carried out the computational analyses; DSC, LASC, RD, JL and NAR interpreted the results obtained; DSC and NAR wrote the paper; DSC, LASC, RD, JL and NAR revised and corrected the manuscript.

Declaration of Competing Interest

The authors declare no conflict of interest relevant in the context of the present work.

Acknowledgements

This study was financed in part by the Coordenação de Aperfeiçoamento de Pessoal de Nível Superior - Brazil (CAPES) – Finance Code 001. DSC is thankful to CAPES, as well as to Conselho Nacional de Desenvolvimento Científico e Tecnológico – Brazil (CNPq) for the doctorate fellowships granted. NAR wishes to thank Fundação Carlos Chagas Filho de Amparo à Pesquisa do Estado do Rio de Janeiro – Brazil (FAPERJ) and CNPq for the research fellowships awarded. NAR and JL also thank FAPERJ (grant number E-26/010.001838/2015) for specifically supporting this project. The authors are grateful for the Laboratório Multiusuário de Difração de Raios-X (Universidade Federal de Juiz de Fora – Brazil) for the XRD facilities. RD is thankful to Fundação de Amparo à Pesquisa do Estado de Minas Gerais – Brazil (FAPEMIG), CNPq and Financiadora de Estudos e Projetos (Finep). LASC thanks CNPq for the research grant 307887/2018–9.

Supplementary materials

Supplementary material associated with this article can be found, in the online version, at doi:10.1016/j.molstruc.2020.129437.

References

[1] J. Brum, T. França, J. Villar, Synthesis and Biological Activity of Hydrazones and Derivatives: a Review, Mini Rev. Med. Chem. 20 (5) (2020) 342–368.
[2] S. Thota, D.A. Rodrigues, P.S.M. Pinheiro, L.M. Lima, C.A.M. Fraga, E.J. Barreiro, N-Acylhydrazones as drugs, Bioorg. Med. Chem. Lett. 28 (17) (2018) 2797–2806.
[3] A. Almasirad, M. Tajik, D. Bakhtiari, A. Shafiee, M. Abdollahi, M.J. Zamani, R. Khorasani, H. Esmaily, Synthesis and analgesic activity of N-Arylhydrazone derivatives of mefenamic acid, J. Pharm. Pharm. Sci. 8 (3) (2005) 419–425.
[4] A. Kajal, S. Bala, N. Sharma, S. Kamboj, V. Saini, Therapeutic potential of hydrazones as anti-inflammatory agents, Int. J. Med. Chem. 2014 (2014) 761030.
[5] F.R. Pavan, P.I.da S. Maia, S.R. Leite, V.M. Deflon, A.A. Batista, D.N. Sato, S.G. Franzblau, C.Q. Leite, Thiosemicarbazones, semicarbazones, dithiocarbazates and hydrazide/hydrazones: anti-Mycobacterium tuberculosis activity and cytotoxicity, Eur. J. Med. Chem. 45 (5) (2010) 1898–1905.
[6] P. Vicini, M. Incerti, I.A. Doytchinova, P. La Colla, B. Busonera, R. Loddo, Synthesis and antiproliferative activity of benzo[*d*]isothiazole hydrazones, Eur. J. Med. Chem. 41 (5) (2006) 624–632.
[7] S. Sarkar, A.A. Siddiqui, S.J. Saha, R. De, S. Mazumder, C. Banerjee, M.S. Iqbal, S. Nag, S. Adhikari, U. Bandyopadhyay, Antimalarial Activity of Small-Molecule Benzothiazole Hydrazones, Antimicrob. Agents Chemother. 60 (7) (2016) 4217–4228.
[8] E. Becker, D.R. Richardson, Development of novel aroylhydrazone ligands for iron chelation therapy: 2-pyridylcarboxaldehyde isonicotinoyl hydrazone analogs, J. Lab. Clin. Med. 134 (5) (1999) 510–521.
[9] D.R. Richardson, Friedreich's ataxia: iron chelators that target the mitochondrion as a therapeutic strategy? Expert Opin. Inv. Drug 12 (2) (2003) 235–245.
[10] P.V. Bernhardt, P. Chin, P.C. Sharpe, D.R. Richardson, Hydrazone chelators for the treatment of iron overload disorders: iron coordination chemistry and biological activity, Dalton Trans. (30) (2007) 3232–3244.
[11] D. Richardson, P.V. Bernhardt, E.M. Becker, Iron chelators and uses thereof, US6989397 B1, 2006.
[12] A.C. González-Baró, R. Pis-Diez, B.S. Parajón-Costa, N.A. Rey, Spectroscopic and theoretical study of the o-vanillin hydrazone of the mycobactericidal drug isoniazid, J. Mol. Struct. 1007 (2012) 95–101.
[13] L.V. de Freitas, C.C. da Silva, J. Ellena, L.A. Costa, N.A. Rey, Structural and vibrational study of 8-hydroxyquinoline-2-carboxaldehyde isonicotinoyl hydrazone–a potential metal-protein attenuating compound (MPAC) for the treatment of Alzheimer's disease, Spectrochim. Acta A Mol. Biomol. Spectrosc. 116 (2013) 41–48.
[14] R.A. Hauser-Davis, L.V. de Freitas, D.S. Cukierman, W.S. Cruz, M.C. Miotto, J. Landeira-Fernandez, A.A. Valiente-Gabioud, C.O. Fernández, N.A. Rey, Disruption of zinc and copper interactions with Aβ(1-40) by a non-toxic, isoniazid-derived, hydrazone: a novel biometal homeostasis restoring agent in Alzheimer's disease therapy? Metallomics 7 (2015) 743–747.
[15] V.d.S. Nogueira, M.C.Ramalho Freitas, W.S. Cruz, T.S. Ribeiro, J.A.L.C. Resende, N.A. Rey, Structural and spectroscopic investigation on a new potentially bioactive di-hydrazone containing thiophene heterocyclic rings, J. Mol. Struct. 1106 (2016) 121–129.
[16] R.S. Moraes, R.E. Aderne, M. Cremona, N.A. Rey, Luminescent properties of a di-hydrazone derived from the antituberculosis agent isoniazid: potentiality as an emitting layer constituent for OLED fabrication, Opt. Mater. 52 (2016) 186–191.
[17] A.C. González-Baró, V. Ferraresi-Curotto, R. Pis-Diez, B.S. Parajón Costa, J.A.L.C. Resende, F.C.S. de Paula, E.C. Pereira-Maia, N.A. Rey, A novel oxidovanadium(V) compound with an isonicotinohydrazide ligand. A combined experimental and theoretical study and cytotoxity against K562 cells, Polyhedron-Polyhedron 135 (2017) 303–310.
[18] D.S. Cukierman, A.B. Pinheiro, S.L. Castiñeiras-Filho, A.S. da Silva, M.C. Miotto, A. De Falco, T. de, P. Ribeiro, S. Maisonette, A.L. da Cunha, R.A. Hauser-Davis, J. Landeira-Fernandez, R.Q. Aucélio, T.F. Outeiro, M.D. Pereira, C.O. Fernández, N.A. Rey, A moderate metal-binding hydrazone meets the criteria for a bioinorganic approach towards Parkinson's disease: therapeutic potential, blood-brain barrier crossing evaluation and preliminary toxicological studies, J. Inorg. Biochem. 170 (2017) 160–168.
[19] D.S. Cukierman, E. Accardo, R.G. Gomes, A. De Falco, M.C. Miotto, M.C.R. Freitas, M. Lanznaster, C.O. Fernández, N.A. Rey, Aroylhydrazones constitute a promising class of 'metal-protein attenuating compounds' for the treatment of Alzheimer's disease: a proof-of-concept based on the study of the interactions between zinc(II) and pyridine-2-carboxaldehyde isonicotinoyl hydrazone, J. Biol. Inorg. Chem. 23 (8) (2018) 1227–1241.
[20] D.S. Cukierman, N. Bodnár, B.N. Evangelista, L. Nagy, C. Kállay, N.A. Rey, Impact of pyridine-2-carboxaldehyde-derived aroylhydrazones on the copper–catalyzed oxidation of the M112A PrP, J. Biol. Inorg. Chem. 24 (8) (2019) 1231–1244.
[21] J.P. Rada, B.S.M. Bastos, L. Anselmino, C.H.J. Franco, M. Lanznaster, R. Diniz, C.O. Fernández, M. Menacho-Márquez, A.M. Percebom, N.A. Rey, Binucleating Hydrazonic Ligands and Their μ-Hydroxodicopper(II) Complexes as Promising Structural Motifs for Enhanced Antitumor Activity, Inorg. Chem. 58 (13) (2019) 8800–8819.
[22] J.P. Rada, J. Forté, G. Gontard, V. Corcé, M. Salmain, N.A. Rey, Isoxazole-Derived Aroylhydrazones and Their Dinuclear Copper(II) Complexes Show Antiproliferative Activity on Breast Cancer Cells with a Potentially Alternative Mechanism Of Action, Chem. Bio. Chem. (2020) in press.
[23] D.S. Cukierman, D.F. Lázaro, P. Sacco, P.R. Ferreira, R. Diniz, C.O. Fernández, T.F. Outeiro, N.A. Rey, X1INH, an improved next-generation affinity-optimized hydrazonic ligand, attenuates abnormal copper(I)/copper(II)-α-Syn interactions and affects protein aggregation in a cellular model of synucleinopathy, Dalton Trans. (2020) in press.
[24] S. Wertz, D. Leifert, A. Studer, Cross dehydrogenative coupling via base-promoted homolytic aromatic substitution (BHAS): synthesis of fluorenones and xanthones, Org. Lett. 15 (4) (2013) 928–931.
[25] Y.-.P. Zhang, Y.-.C. Jiao, Y.-.S. Yang, C.-.L. Li, Ligand-free catalytic system for the synthesis of diarylethers over Cu_2O/Cu-CNTs as heterogeneous reusable catalyst, Tetrahedron Lett. 54 (48) (2013) 6494–6497.
[26] O. Rigaku, CrysAlis PRO. Rigaku Oxford Diffraction, Yarnton, England (2015).
[27] M.C. Burla, R. Caliandro, B. Carrozzini, G.L. Cascarano, C. Cuocci, C. Giacovazzo, M. Mallamo, A. Mazzone, G. Polidori, Crystal structure determination and refinement via SIR2014, J. Appl. Crystallogr. 48 (1) (2015) 306–309.
[28] G.M. Sheldrick, Crystal structure refinement with SHELXL, Acta Crystallogr. C Struct. Chem. 71 (Pt 1) (2015) 3–8.
[29] L.J. Farrugia, WinGX and ORTEP for Windows: an update, J. Appl. Crystallogr. 45 (4) (2012) 849–854.
[30] C. Barnes, ORTEP-3 for Windows - a version of ORTEP-III with a Graphical User Interface (GUI) by J. Farrugia, J. Appl. Crystallogr. 30 (5 Part 1) (1997) 568.
[31] POV-Ray for Windows – Version 3.7.0.msvc10.win64. Persistence of Vision Raytracer Pty, Ltd (2013).
[32] C.F. Macrae, I.J. Bruno, J.A. Chisholm, P.R. Edgington, P. McCabe, E. Pidcock, L. Rodriguez-Monge, R. Taylor, J. Van De Streek, P.A. Wood, Mercury CSD 2.0–new features for the visualization and investigation of crystal structures, J. Appl. Crystallogr. 41 (2) (2008) 466–470.
[33] M. Turner, J. McKinnon, S. Wolff, D. Grimwood, P. Spackman, D. Jayatilaka, M. Spackman, Crystal Explorer 17, The University of Western Australia, Perth, WA, Australia, 2017.
[34] R. Sure, S. Grimme, Corrected small basis set Hartree-Fock method for large systems, J. Comp. Chem. 34 (19) (2013) 1672–1685.
[35] H. Kruse, S. Grimme, A geometrical correction for the inter- and intra-molecular basis set superposition error in Hartree-Fock and density functional theory calculations for large systems, J. Chem. Phys. 136 (15) (2012) 154101.
[36] S. Grimme, S. Ehrlich, L. Goerigk, Effect of the damping function in dispersion corrected density functional theory, J. Comput. Chem. 32 (7) (2011) 1456–1465.
[37] S. Grimme, J. Antony, S. Ehrlich, H. Krieg, A consistent and accurate ab initio parametrization of density functional dispersion correction (DFT-D) for the 94 elements H-Pu, J. Chem. Phys. 132 (15) (2010) 154104.

[38] F. Neese, ORCA: an Ab initio, Density Functional and Semiempirical Program Package, Ver. 3.0.3, Max Planck Institute for Bioinorganic Chemistry, Germany, 2011.
[39] T. Yanai, D.P. Tew, N.C. Handy, A new hybrid exchange–correlation functional using the Coulomb-attenuating method (CAM-B3LYP), Chem. Phys. Lett. 393 (1) (2004) 51–57.
[40] R. Ditchfield, W.J. Hehre, J.A. Pople, Self-Consistent Molecular-Orbital Methods. IX. An Extended Gaussian-Type Basis for Molecular-Orbital Studies of Organic Molecules, J. Chem. Phys. 54 (2) (1971) 724–728.
[41] G.W.T.M.J. Frisch, H.B. Schlegel, G.E. Scuseria, M.A. Robb, J. R., G.S. Cheeseman, V. Barone, G.A. Petersson, H. Nakatsuji, X. Li, M., A.M. Caricato, J. Bloino, B.G. Janesko, R. Gomperts, B. Mennucci, H.J.V.O.P. Hratchian, A.F. Izmaylov, J.L. Sonnenberg, D. Williams-Young, F.L.F. Ding, F. Egidi, J. Goings, B. Peng, A. Petrone, T. Henderson, V.G.Z.D. Ranasinghe, J. Gao, N. Rega, G. Zheng, W. Liang, M. Hada, K.T.M. Ehara, R. Fukuda, J. Hasegawa, M. Ishida, T. Nakajima, Y. Honda, H.N.O. Kitao, T. Vreven, K. Throssell, J.A. Montgomery Jr., J. E., F.O. Peralta, M. Bearpark, J.J. Heyd, E. Brothers, K.N. Kudin, V. N., T.K. Staroverov, R. Kobayashi, J. Normand, K. Raghavachari, A. Rendell, J.S.S.I.C. Burant, J. Tomasi, M. Cossi, J.M. Millam, M. Klene, C., R.C. Adamo, J.W. Ochterski, R.L. Martin, K. Morokuma, O. Farkas, J. B., D.J.F. Foresman, Gaussian 09 Revision D.01, Gaussian Inc, Wallingford CT, 2013.
[42] Z.-.Q. Lei, H. Li, Y. Li, X.-.S. Zhang, K. Chen, X. Wang, J. Sun, Z.-J. Shi, Extrusion of CO from Aryl Ketones: rhodium(I)-Catalyzed C-C Bond Cleavage Directed by a Pyridine Group, Angew Chem. Int. Ed. Engl. 51 (11) (2012) 2690–2694.
[43] H. Li, Y. Li, X.S. Zhang, K. Chen, X. Wang, Z.J. Shi, Pyridinyl directed alkenylation with olefins via Rh(III)-catalyzed C-C bond cleavage of secondary arylmethanols, J. Am. Chem. Soc. 133 (39) (2011) 15244–15247.
[44] M.A. Spackman, D. Jayatilaka, Hirshfeld surface analysis, Cryst. Eng. Comm. 11 (1) (2009) 19–32.
[45] M.A. Spackman, J.J. McKinnon, Fingerprinting intermolecular interactions in molecular crystals, Cryst. Eng. Comm. 4 (66) (2002) 378–392.
[46] M.J. Turner, S.P. Thomas, M.W. Shi, D. Jayatilaka, M.A. Spackman, Energy frameworks: insights into interaction anisotropy and the mechanical properties of molecular crystals, Chem. Comm. 51 (18) (2015) 3735–3738.